Available online at www.sciencedirect.com
SCIENCE DIRECT®
Polymer 44 (2003) 7427–7440
polymer
www.elsevier.com/locate/polymer

Compatibilizing effect of maleated polypropylene on the mechanical properties and morphology of injection molded polyamide 6/polypropylene/organoclay nanocomposites

W.S. Chow[a], Z.A. Mohd Ishak[a,*], J. Karger-Kocsis[b], A.A. Apostolov[c], U.S. Ishiaku[d]

[a]*School of Materials and Mineral Resources Engineering, Engineering Campus, Universiti Sains Malaysia, Seri Ampangan 14300 Nibong Tebal, Penang, Malaysia*
[b]*Institute for Composite Materials Ltd, University of Kaiserslautern, P.O. Box 3049, D-67663 Kaiserslautern, Germany*
[c]*Laboratory on Structure and Properties of Polymers, Sofia University, BG-1126 Sofia, Bulgaria*
[d]*Advanced Fibro-Science, Kyoto Institute of Technology, Matsugasaki, Sakyo-ku, Kyoto 606-8585, Japan*

Received 21 April 2003; received in revised form 19 August 2003; accepted 1 September 2003

Abstract

Polyamide 6/polypropylene (PA6/PP = 70/30 parts) blends containing 4 phr (parts per hundred resin) of organophilic modified montmorillonite (organoclay) were prepared using twin screw extruder followed by injection molding. Maleated polypropylene (MAH-g-PP) was used to compatibilize the blend system. The mechanical properties of PA6/PP nanocomposites were studied through tensile and flexural tests. Scanning electron microscopy (SEM) and transmission electron microscopy (TEM) were used to assess the fracture surface morphology and the dispersion of the organoclay, respectively. X-ray diffraction (XRD) was used to characterize the formation of nanocomposites. The thermal properties were characterized by using differential scanning calorimetry (DSC) and thermogravimetric analysis (TGA). The dynamic mechanical properties of PA6/PP nanocomposites were analyzed by using dynamic mechanical thermal analyzer (DMTA). The strength and stiffness of PA6/PP nanocomposites were improved significantly in the presence of MAH-g-PP. This has been attributed to the synergistic effect of organoclay and MAH-g-PP. The MAH-g-PP compatibilized PA6/PP nanocomposites showed a homogeneous morphology supporting the compatibility improvement between PA6, PP and organoclay. TEM and XRD results revealed the formation of nanocomposites as the organoclay was intercalated and exfoliated. A possible chemical interaction between PA6, PP, organophilic modified montmorillonite and MAH-g-PP was proposed based on the experimental work.

Keywords: Polyamide 6/polypropylene blends; Nanocomposites; Organoclay

1. Introduction

The achievement of compatibilization, whether by addition of a third component (i.e. compatibilizer) or by in situ chemical reaction between blend components (reactive blending), has played an important role in the development of polymer blends [1]. Polyamide (PA6) and polypropylene (PP) blending has been attempted to achieve improvement in mechanical properties, paintability and barrier properties, where PA6 contribute mechanical and thermal properties, while PP ensures good processability and insensitivity to moisture [2].

In recent years, polymer nanocomposites have attracted great interest. These nanocomposites exhibit superior properties such as enhanced mechanical properties, reduced gas permeability, and improved flame retardancy [3]. Polymer-layered silicate nanocomposites are currently prepared in four ways: in situ polymerization, intercalation from a polymer solution, direct intercalation by molten polymer and sol–gel technology [4]. Direct polymer melt intercalation is the most attractive because of its low cost, high productivity and compatibility with current polymer processing techniques [5]. Numerous researchers described polymer–clay nanocomposites based on single polymer matrix [6–31]. However, thermoplastic nanocomposites based on blends of two or more polymeric materials, i.e. binary or ternary blends, seem to be a new approach in the

* Corresponding author. Tel.: +60-4-593-7788; fax: +60-4-594-1011.
E-mail address: zarifin@eng.usm.my (Z.A. Mohd Ishak).

0032-3861/$ - see front matter © 2003 Elsevier Ltd. All rights reserved.
doi:10.1016/j.polymer.2003.09.006

nanocomposites studies. The work presented in this paper focuses on the study of thermoplastic nanocomposites based on blends of PA6 and PP.

In a previous study on the PA6/PP nanocomposites [32], the effect of organoclay loading from 2 up to 10 phr on the tensile and flexural properties was reported. Organoclay of 4 phr has been observed to be the optimum loading for PA6/PP blends. X-ray diffraction (XRD) results revealed that the organoclay was intercalated/exfoliated in the PA6/PP nanocomposites. However, the enhancement in the mechanical properties due to the presence of organoclay was rather limited. This was traced to two main factors: the lack of interaction between the organoclay and PP component and missing compatibility between the major and minor phases (i.e. PA6 and PP, respectively). Thus, it was expected that the mechanical properties and compatibility of PA6/PP blends could be further enhanced by using a suitable compatibilizer, such as maleated polypropylene (MAH-g-PP) [33]. Therefore, this work was devoted to study the morphology dependent mechanical behavior of injection molded compatibilized nanocomposites based on PA6/PP blends.

2. Experimental

2.1. Materials

The PA6 (Amilan CM 1017) used in this study was a commercial product from Toray Nylon Resin AMILAN, Japan. The melt flow index (MFI at 230 °C and 2.16 kg load) and density of PA6 were 35 g/10 min and 1.14 g/cm^3, respectively. PP (Pro-Fax SM-240) was supplied by Titan Himont Polymer (M) Sdn. Bhd. MFI and density of PP is 25 g/10 min (at 230 °C and 2.16 kg load) and 0.9 g/cm^3, respectively. MAH-g-PP (Polybond 3200) with 1.2 wt% of maleic anhydride (MA) was supplied by Uniroyal Chemical, Middlebury. The MFI of MAH-g-PP is 105 g/10 min at 190 °C and 2.16 kg load. Organoclay (Nanomer 1.30TC) was a commercial product from Nanocor, Inc., USA. This organoclay is a white powder containing montmorillonite (70 wt%) intercalated by octadecylamine (30 wt%). Mean dry particle size of the organoclay is 16–22 μm. The designation, composition and density value of the materials tested is given in Table 1.

Table 1
Materials designation, compositions and densities

Designation	Composition	Parts	Density (g/cm^3)
PA6/PP	PA6/PP	70/30	0.95
PA6/PP/5M	PA6/PP/MAH-g-PP	70/30/5	1.03
PA6/PP/10M	PA6/PP/MAH-g-PP	70/30/10	1.02
PA6/PP/4TC	PA6/PP/organoclay	70/30/4	1.03
PA6/PP/5M/4TC	PA6/PP/MAH-g-PP/organoclay	70/30/5/4	1.06
PA6/PP/10M/4TC	PA6/PP/MAH-g-PP/organoclay	70/30/10/4	1.05

2.2. Specimen preparation

Melt compounding of the PA6/PP (70/30) blends and nanocomposites were done on counter-rotating twin screw extruder (Berstoff). The extrusion zone temperature ranged from 220 to 230 °C. Prior to extrusion, PA6 pellets and organoclay were dehumidified by using a vacuum oven at 80 °C for 8 h. The extrudates were pelletized with the Haake pelletizer. The pellets were injection molded into standard tensile bar using a Niigata AN 50 injection molding machine. Injection molding temperature ranged from 225 to 240 °C. Prior to injection molding, all pellets were dehumidified in vacuum oven (80 °C for 8 h). The tensile test specimen was molded in Type I according to ASTM D 638.

2.3. Mechanical properties

Tensile test was carried out with an Instron-5582 machine at 23 °C, according to ASTM D638, at a crosshead speed of 50 mm/min. *E*-modulus, tensile strength and elongation at break were evaluated from the stress–strain data. Flexural measurements were carried out according to ASTM D790 using 3-point bending configuration at 3 mm/min deformation rate.

2.4. Melt flow index (MFI) and density measurement

Melt flow index and density of various materials was measured by using Melt Flow Indexer (at 230 °C, load 2.16 kg) and density balance (model Precisa XT 220 A).

2.5. Molau's test

The pellets of uncompatibilized and MAH-g-PP compatibilized PA6/PP nanocomposites were immersed in concentrated formic acid in order to check the compatibility of the blend. Note that the more stable is the related solution the better the compatibility between the blend components is.

2.6. Microscopic examination (SEM and TEM)

The fracture surface of selected PA6/PP based nanocomposites was inspected in a scanning electron microscope (SEM; Leica Cambrige Ltd model S 360). The fracture surface were gold coated to avoid electrostatic charging during examination. Transmission electron microscopy (TEM) measurements were carried out with a LEO 912 Omega transmission electron microscope applying an acceleration voltage of 120 keV. The specimens were prepared using an Ultracut E (Reichert and Jung) ultra-

microtome. Thin sections of about 100 nm thickness were cut with a Diatome diamond knife at room temperature.

2.7. Energy dispersive X-ray microanalysis system (EDX)

EDX (EDAX Falcon System) was used to analyse the occurrence of elements in the specimens that sputtered with gold.

2.8. Infrared spectroscopic analysis

Fourier-transform infrared spectroscopy (FTIR; Nicolet, Avator® 360) was used to obtain some qualitative information about the functional groups and chemical characteristics of the organoclay. FTIR spectra were obtained from KBr pellets at room temperature. FTIR spectra were taken also of PA6/PP nanocomposites with and without MAH-g-PP compatibilizer.

2.9. X-ray diffraction (XRD)

Wide-angle X-ray spectra were recorded with a D 500 diffractometer (Siemens) in step scan mode using Ni-filtered Cu Kα radiation (0.1542 nm wavelength). Powder samples were scanned in reflection, whereas the injection-molded compounds were scanned in transmission in the interval of $2\Theta = 2-10°$. The interlayer spacing of the organoclay was derived from the peak position (d_{001}-reflection) in the XRD diffractograms according to the Bragg equation.

2.10. Dynamic-mechanical thermal analysis (DMTA)

The complex modulus (E^*), its storage (E') and loss parts (E'') and the mechanical loss factor ($\tan\delta = E''/E'$) as a function of temperature (T), were assessed by dynamic mechanical thermal analysis (DMTA) using an Eplexor 25N device of Gabo Qualimeter, Germany. DMTA spectra were taken in tension mode at 10 Hz frequency in a broad temperature range ($T = -110$ to $+230$ °C). The DMTA device operated under load control by setting 50 N as static and ±25 N as dynamic load.

2.11. Thermal analysis (DSC and TGA)

The melting and crystallization behavior of the blends and nanocomposites were studied under nitrogen atmosphere by differential scanning calorimetry (Perkin Elmer DSC-6), using 8–10 mg sample sealed into aluminum pans. In order to avoid any effect of moisture, all the test specimens were dried using vacuum oven at 80 °C prior to the measurements. The temperature was raised from 50 to 250 °C at a heating rate of 10 °C/min, and after a period of 5 min it was swept back at −10 °C/min. Second heating similar to the first was then performed in order to erase the thermal history. The melting thermogram was recorded from the second heating. The percent crystallinity was calculated by using a ΔH_f^0(PA6) = 190.8 J/g and ΔH_f^0(PP) = 209.2 J/g. Thermogravimetry analysis (TGA) was performed with a Perkin Elmer TGA 7 thermal analysis system. The TGA scans were recorded at 10 °C/min under a nitrogen atmosphere from 50 to 600 °C.

3. Results and discussion

3.1. Melt flow index (MFI)

The MFI value of PA6/PP blends decreased in the presence of MAH-g-PP—see Table 2. This may be attributed to the higher reactivity of MAH resulting in the formation of a graft copolymer, viz. PA6-g-PP in the blends [34]. The intermolecular bonding in the copolymer may restrict the movement of the polymeric chains in the PA6/PP blends, thus affecting the melt viscosity. When MAH-g-PP was added to PA6/PP blends, the anhydride group of MAH would react with the terminal amino group of PA6 during melt mixing to form PA6-g-PP copolymer [33,38]. Note that numerous researchers studied the effect of compatibilizers (e.g. MAH-g-PP) on the properties of PA6/PP blends [33–44]. The incorporation of MAH-g-PP in the PA6/PP/organoclay nanocomposites slightly decreased the MFI of the respective blends (cf. Table 2). This may be attributed to the interaction between the amine group of the intercalant in the organoclay and anhydride group of the MAH-g-PP. Another possible interaction is between the organoclay and PA6: the NH_2 group in the octadecylamine is believed to be compatible with PA6 and is capable of forming hydrogen bonds as shown later. These interactions reduce the chain mobility and yield lower MFI values.

3.2. Density

Table 1 also lists the densities of various PA6/PP blends and composites. The densities of all filled and compatibilized PA6/PP are higher than the unfilled counterparts. As expected, the incorporation of organoclay increases the density of both uncompatibilized and compatibilized PA6/PP blends.

3.3. Mechanical properties

The addition of MAH-g-PP in the PA6/PP blends mildly affected the tensile E-modulus. However, the addition of organoclay increases the stiffness of the uncompatibilized PA6/PP blends significantly—see Table 2. Note that a stiffness increase can be caused by both reinforcing and non-reinforcing fillers. The organoclay is able to act as reinforcing filler due to its high aspect ratio and platelet structure. The enhancement in the E-modulus of PA6/PP nanocomposites became more significant with the incorporation of the MAH-g-PP (cf. Table 2). This is believed to be associated with the functionality of the organoclay which

Table 2
MFI and mechanical properties of the compositions

Properties	Compositions					
	PA6/PP	PA6/PP/4TC	PA6/PP/5M	PA6/PP/5M/4TC	PA6/PP/10M	PA6/PP/10M/4TC
MFI (g/10 min)	50.4	38.9	13.4	9.6	12.1	8.2
Tensile						
E-modulus (GPa)	1.87	2.11	1.93	2.38	1.89	2.30
Yield stress (MPa)	38.6	39.0	45.2	50.1	42.8	49.4
Ultimate strength (MPa)	32.1	38.0	29.2	49.6	25.2	48.5
Elongation at break (%)	22.8	4.2	32.5	4.8	38.8	5.3
Flexural						
E-modulus (GPa)	1.73	1.99	1.60	2.12	1.56	2.02
Strength (MPa)	76.2	78.7	80.1	98.0	77.5	88.4

promotes the interaction between the organoclay and PA6/PP matrix. The possible mechanism of this interaction will be discussed later.

The incorporation of the MAH-g-PP increased the yield stress of the PA6/PP blends significantly (cf. Table 2). When MAH-g-PP was added to the PA6/PP blend, a PA6-g-PP copolymer formed which strongly improved the interfacial adhesion between PA6 and PP and most likely affected the morphology of the blends. However, with 10 phr of MAH-g-PP, the yield stress decreased slightly due to the plasticization effect of low molecular weight MAH-g-PP. According to Sathe et al. [34,35], up to a saturation level of the compatibilizer, its molecules are located in the interphase between the matrix and the dispersed phase. However, when the concentration of a compatibilizer is above the saturation level, only a part of the molecules locates in the interfacial area, and the excess is dispersed in the matrix affecting its homogeneity and consequently the mechanical properties of the blends. The incorporation of 4 phr organoclay in PA6/PP blends did not enhance the yield stress of the composites significantly. However, in the presence of MAH-g-PP of either 5 or 10 phr, the yield stress of the PA6/PP/organoclay nanocomposites was well improved (cf. Table 2).

The data in Table 2 also demonstrate the effect of MAH-g-PP on the tensile strength and elongation at break of the compounds. The results indicate that with increasing concentration of MAH-g-PP the tensile strength of the PA6/PP blends slightly decreased. Tensile strength of the uncompatibilized PA6/PP blends increased moderately when filled with 4 phr organoclay. The tensile strength of the PA6/PP/organoclay nanocomposites increased significantly with the addition of the compatibilizer. This improvement may be attributed to the platelet structure and related anisotropy when the layers of organoclay are delaminated. Delamination (i.e. intercalation and exfoliation) of the layered silicate could also affect the crystallinity and polymorphism in both PA6 and PP. Delamination of the layered organoclay is favored by the shear forces during extrusion compounding and injection molding.

Note that the ductility (i.e. elongation at break) of the PA6/PP blends increased with the addition of MAH-g-PP (cf. Table 2). The specimens showed increased necking and the formation of a prominent fibrillar fracture surface when MAH-g-PP was added to the PA6/PP blends. This indicated the formation of PA6-g-PP copolymer, which strengthened the interface between the PA6 and PP phases. Subsequently, the compatibilized PA6/PP blends could withstand the tensile deformation to a higher elongation and thus failed after necking. The addition of organoclay caused a tremendous drop in the elongation at break of both compatibilized and non-compatibilized PA6/PP blends (cf. Table 2). Note that the tensile fracture behavior of polymers is rather complex [45]. Brittle fracture could be observed for both uncompatibilized and compatibilized PA6/PP/organoclay nanocomposites. PA6 and compatibilized PA6/PP blends showed ductile fracture after necking, whereas uncompatibilized PA6/PP blends and all organoclay filled PA6/PP nanocomposites exhibited brittle fracture without necking.

Data in Table 2 also highlight the effect of MAH-g-PP on the flexural E-modulus and strength of the PA6/PP blends and related nanocomposites. The addition of MAH-g-PP has slightly reduced the flexural modulus of the PA6/PP blends. This trend resembles to that of the tensile modulus. The addition of MAH-g-PP in the PA6/PP blends increase the flexural strength, albeit not significantly. A similar trend to that of the tensile strength was again observed for the flexural strength whereby the related enhancement is more prominent in blends compatibilized with 5 phr than by 10 phr MAH-g-PP. This suggests that a given loading of MAH-g-PP is required to obtain PA6/PP blends of optimum properties, which was in line with the prediction of Sathe et al. [34]. The incorporation of organoclay did improved the flexural properties of the uncompatibilized and MAH-g-PP compatibilized PA6/PP blends—cf. Table 2.

A possible chemical interaction between PA6, PP and MAH-g-PP is proposed in Fig. 1. In the presence of MAH-g-PP, a PA6-g-PP copolymer might have resulted. According to Ide and Hasegawa [33], Sathe et al. [34] and Coran et al.

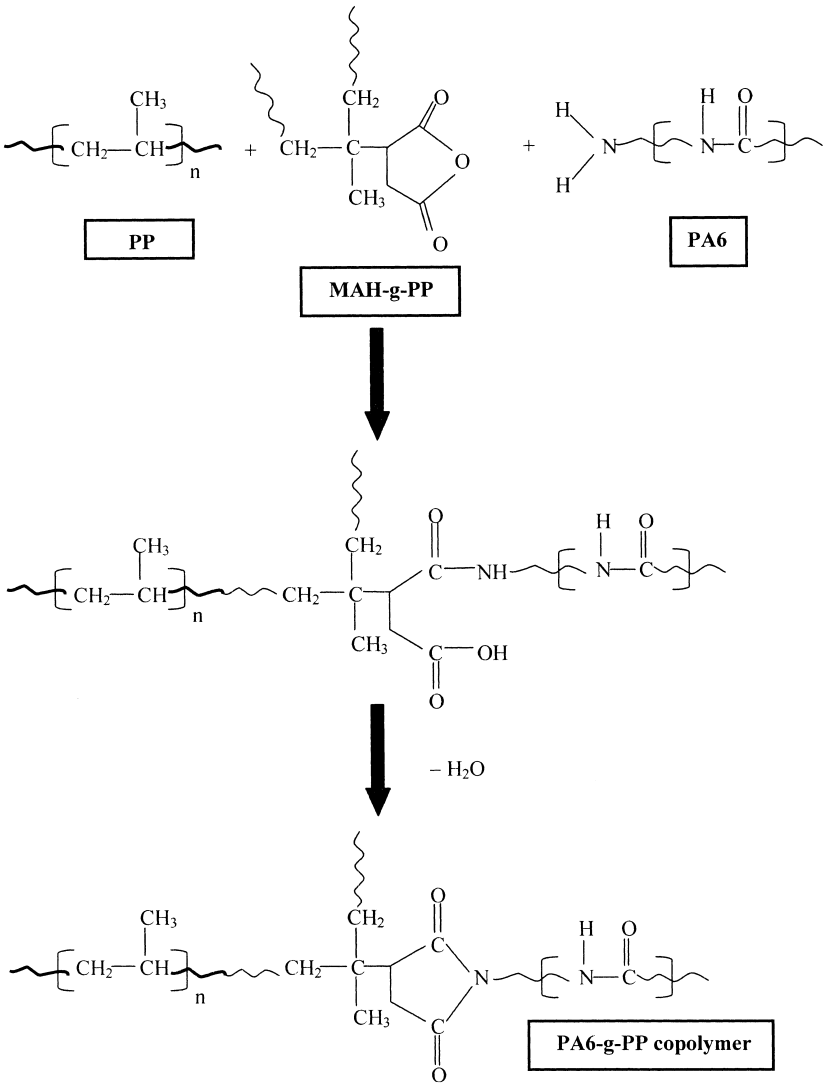

Fig. 1. Possible chemical reactions between PA6, PP and MAH-g-PP.

[38] when MAH-g-PP is added to PA6/PP blends, the anhydride group of MAH reacts with the terminal amino group of PA6 during melt mixing, resulting in the formation of PA6-g-PP copolymer.

Fig. 2 shows the proposed interaction between organoclay and the PA6-g-PP copolymer formed in the presence of MAH-g-PP in the PA6/PP blends. It is believed that hydrogen bonding could form between the amide group of the PA6-g-PP copolymer and the octadecylamine group of the organoclay intercalant. Note that this amide–amine reaction could happen when the organoclay was exfoliated in the PA6/PP matrix, subsequently the octadecylamine (intercalant) is capable to form a chemical linkage with PA6-g-PP copolymer.

3.4. X-ray diffraction

Fig. 3 shows the XRD patterns in the range of $2\theta = 2-10^{\circ}$ for organoclay and uncompatibilized and MAH-g-PP compatibilized PA6/PP nanocomposites. The XRD spectrum of the organoclay exhibits a broad intense peak at around $2\theta = 3.25^{\circ}$ corresponding to a basal spacing of 2.72 nm. The XRD spectra of uncompatibilized and MAH-g-PP compatibilized PA6/PP/organoclay composites do not show a characteristic basal reflection of the organoclay. However, they show a shoulder at $2\theta = 2.85^{\circ}$ superimposed to the intense declining part of the XRD spectra. This is a clear hint that a portion of the organoclay is only intercalated. Wu et al. [52] had reported a similar observation in the case of nylon 1012/clay nanocomposites. The absence of the characteristic clay d_{001} peak indicates the exfoliation of the clay platelets in the nylon 1012 matrix. Similar results also reported by Cho and Paul [13], Hsiao et al. [20] and Yano et al. [22]. XRD spectra of the organoclay filled PA6/PP nanocomposites display a prominent increase in the intensity at lower 2θ values when compared with those of the unfilled blends. This likely reflects that the organoclay used was partly intercalated (and

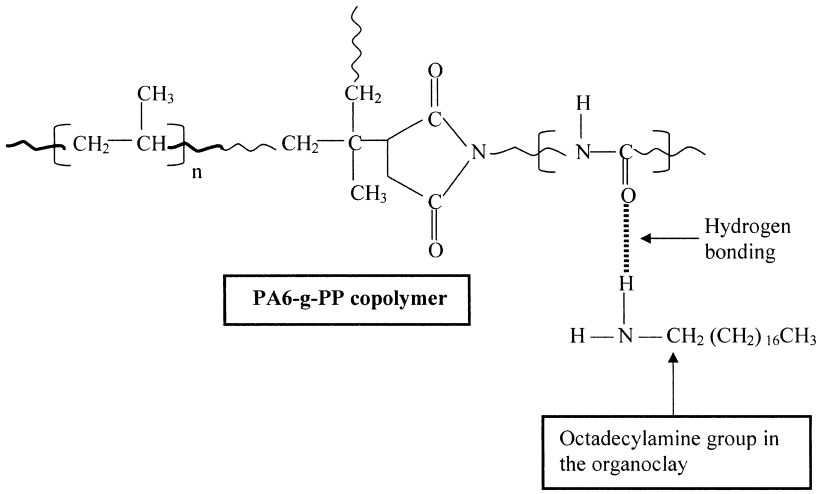

Fig. 2. Proposed interaction between PA6-g-PP copolymer and organoclay.

the related XRD peak lays $2\theta < 2°$) and partly exfoliated. This suggestion will be corroborated later based on SEM and TEM results.

3.5. Thermal properties (TGA and DSC)

TGA curves taken from the organoclay after being subjected to a temperature of 600 °C resulted in 70 wt% ash content. So, the total weight loss of 30 wt% could be attributed to the decomposition of octadecylamine that intercalated into the montmorillonite galleries. The remaining ashes were attributed to the high thermal stability of montmorillonite. This result was in agreement with the data sheets of the organoclay supplier.

The DSC thermograms of PA6/PP blends and related nanocomposites revealed that the melting temperature (T_m) remained unaltered with the addition of either organoclay or MAH-g-PP. However, the crystallization temperature (T_c) for PA6 phase slightly decreased with the incorporation of organoclay and/or MAH-g-PP. Such nucleation effect was often reported for organoclays and compatibilizers. The crystallinity of the PA6 phase increased slightly with addition of organoclay, and the increase was bit more pronounced for MAH-g-PP compatibilized PA6/PP nanocomposites.

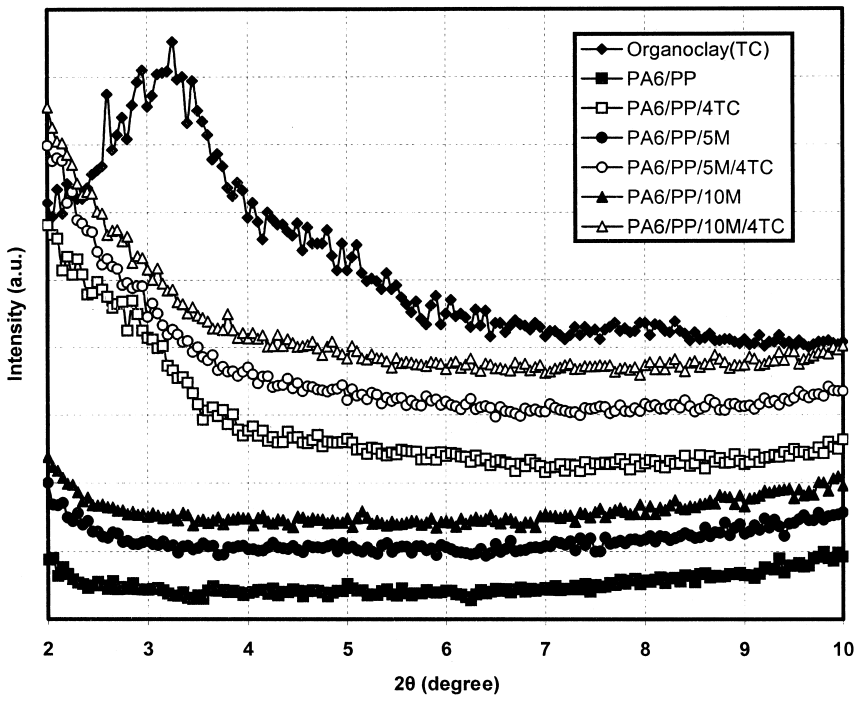

Fig. 3. XRD spectra for the organoclay and PA6/PP nanocomposites.

3.6. Dynamic mechanical thermal properties

The dynamic storage modulus, as well as the tan δ versus temperature traces for the PA6/PP/organoclay systems are shown in Fig. 4(a) and (b). All the curves in Fig. 4(a) show the same pattern, and they can be divided in three main zones: glassy (from -100 to 23 °C), glass–rubber transition (from 23 to 65 °C) and rubbery (from 65 to 200 °C). In the first two zones the storage modulus (E') of the PA6/PP increased with the incorporation of both compatibilizer and organoclay. This is in agreement with the E-moduli from static mechanical tests (Table 2). Incorporation of 4 phr organoclay increased the E' of PA6/PP blends significantly (cf. Fig. 4(a)).

Fig. 4(b) shows the effect of MAH-g-PP on the loss factor (tan δ) for PA6/PP/organoclay systems. Two dynamic relaxation peaks were observed at around 56 °C and -54.8 °C, which referred to as α and β relaxation peaks of PA6, respectively [48–50]. According to Mohd Ishak and Berry [51], the α relaxation peak is believed to be related to the breakage of hydrogen bonding between polymer chain which induces long range segmental chain movement in the amorphous area. This is assigned to the glass transition temperature (T_g) of PA6. The β relaxation peak is related to the segmental amide group in the amorphous area which unattached to the other amide group by hydrogen bonding. The α relaxation peak (T_g) in the tan δ curves for MAH-g-PP compatibilized PA6/PP blends and nanocomposites is

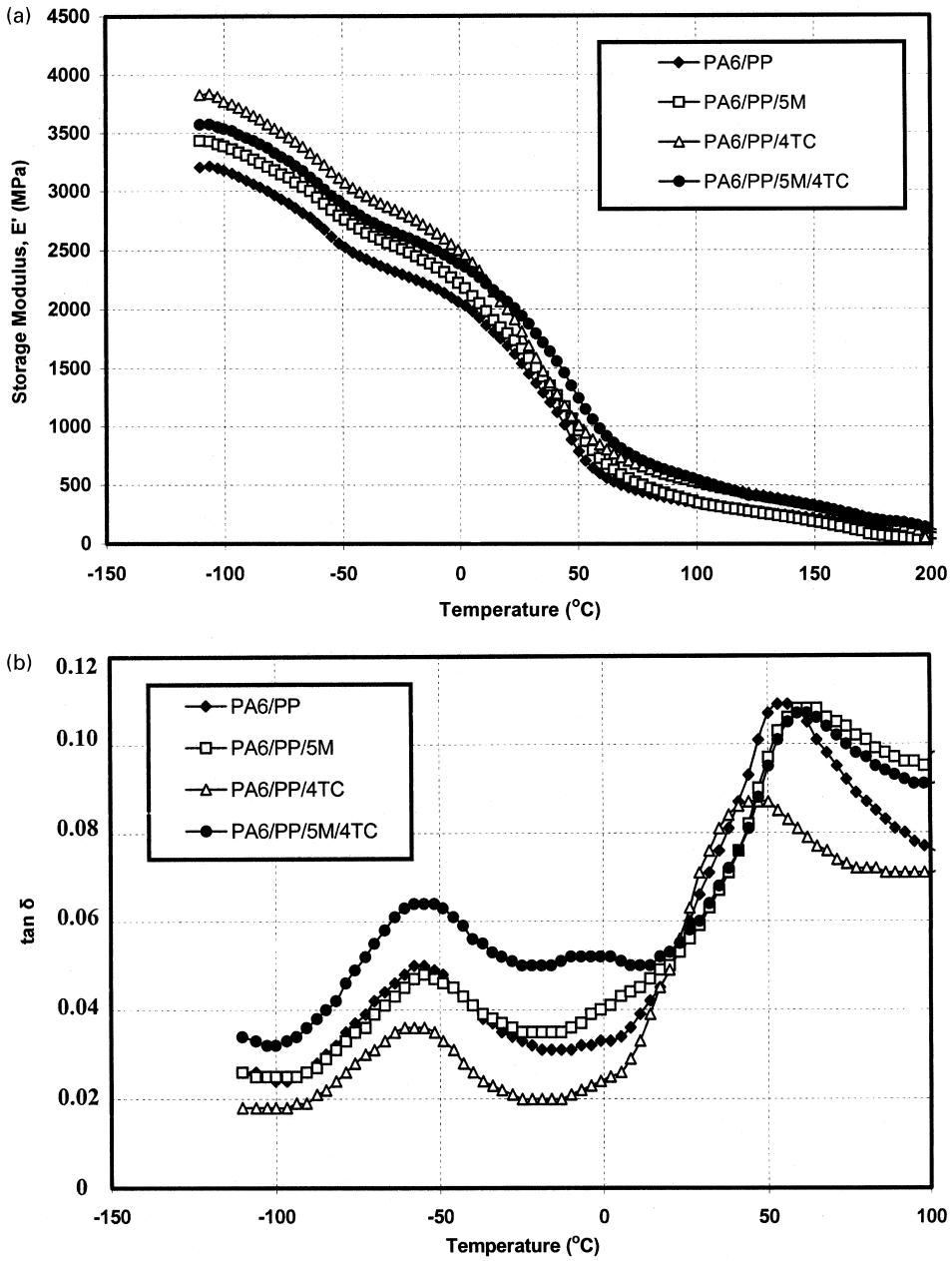

Fig. 4. (a) E' vs T traces for PA6/PP and PA6/PP/organoclay systems. (b) tan δ vs T traces for PA6/PP and PA6/PP/organoclay systems.

higher than the uncompatibilized counter parts. On the other hand, the incorporation of 4 phr organoclay in PA6/PP blends results in a lower α relaxation peak (T_g) if compared to unfilled PA6/PP blends—cf. Fig. 4(b). This suggests that the organoclay became intercalated/exfoliated and a polymer layer formed around the layers. Here, the polymer molecules should have reduced chain mobility as the reinforcing effect of the clay platelets dominates. However, in the presence of MAH-g-PP, the α relaxation peak (T_g) of PA6/PP/organoclay nanocomposites was slightly increased.

3.7. Morphology (SEM and TEM)

SEM micrographs taken from the organoclay particles already indicated that they are prone for easy delamination under shear forces. Recall that delamination of the silicate layers improve the reinforcing efficiency of the organoclay, and subsequently enhances the mechanical properties of the related composites.

Fig. 5 displays a SEM micrograph showing an organoclay particle in the PA6/PP blend. The lay-up of the organoclay particle in this image already reveals some inherent layered structure. Nevertheless, the fact that the organoclay did not change its dimension compared to the initial particle size suggests that it did not exfoliate. Further information was received by using the technique of energy dispersive X-ray analysis. Fig. 6 shows the EDX spectra of the organoclay powder (bottom trace) and PA6/PP/organoclay nanocomposite as depicted in Fig. 5 (top trace). In these EDX spectra, six to seven elements can be observed, i.e. C, O, Mg, Al, Si, Au and Cl. The carbon is due to the octadecylamine intercalant used. Recall that the organoclay contains 30 wt% octadecylamine intercalant. The Au observed in the EDX is associated with the coating material sputtered on the sample. All remaining elements represent

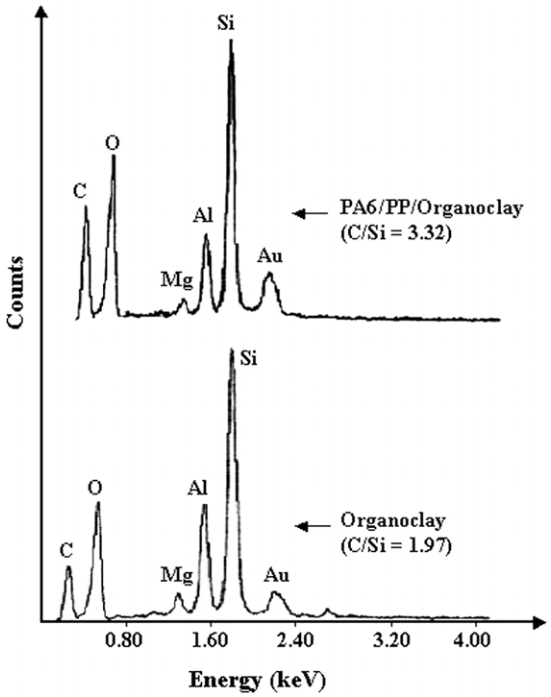

Fig. 6. EDX spectra of the organoclay (bottom) and PA6/PP/organoclay nanocomposite (top).

components of the montmorillonite. Fig. 6 also shows the EDX spectrum of an organoclay particle (see spot size in Fig. 5) in the PA6/PP-based nanocomposite. The carbon content based on the C/Si ratio in the nanocomposite was, however, higher than that of the initial organoclay (cf. Fig. 6). This can be ascribed to some intercalation of the organoclay either with PP or with PA chains.

Fig. 7(a) and (b) shows TEM micrographs of the compatibilized PA6/PP/organoclay nanocomposites containing 5 phr (Fig. 7(a)) and 10 phr MAH-g-PP (Fig. 7(b)), respectively. The dark lines represent the thickness of

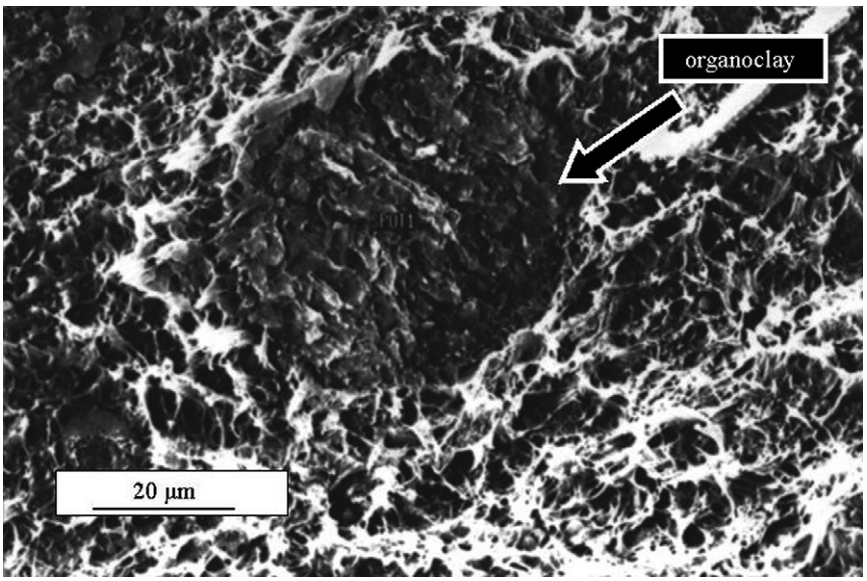

Fig. 5. SEM micrograph showing an organoclay particle in the PA6/PP blend.

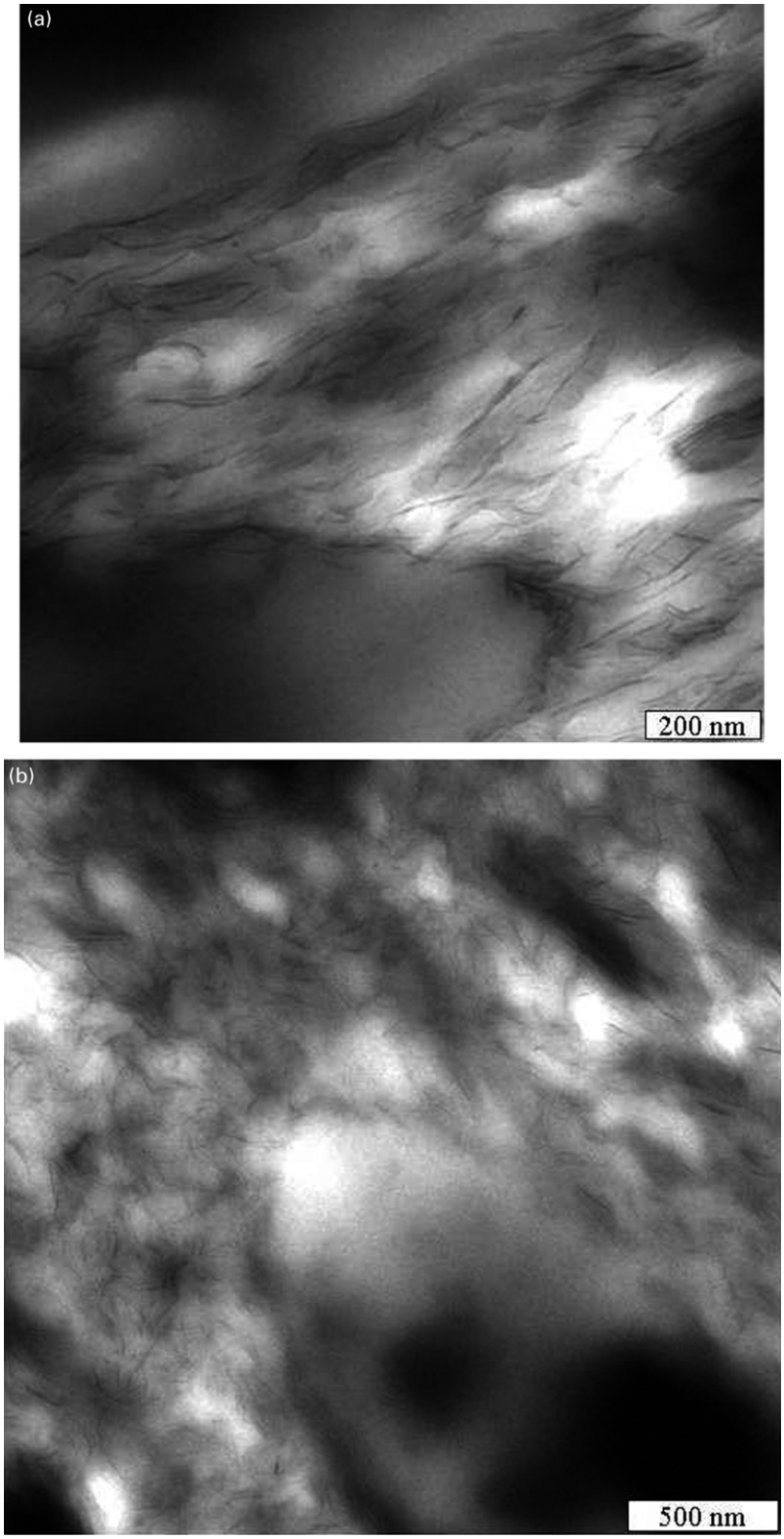

Fig. 7. (a) TEM micrograph taken from the compatibilized PA6/PP/organoclay nanocomposite containing 5 phr of MAH-g-PP. (b) TEM micrograph taken from the compatibilized PA6/PP/organoclay nanocomposite containing 10 phr of MAH-g-PP.

individual clay layers or their agglomerates (tactoids). In our previous work, on PA6/PP/nanocomposites containing 4 phr organoclay, it was found that the organoclay was partly intercalated/exfoliated [32]. Further, the organoclay had a strong tendency to be located in the PA6 phase. In the present work, owing to the presence of MAH-g-PP, a more pronounced exfoliation of the organoclay can be noticed. This may be attributed to the interaction of the MAH-g-PP with the amine groups tethered to the clay layers in the organoclay. As discussed above, in the presence of MAH-g-PP, a graft copolymer, viz. PA6-g-PP should develop. This can be confirmed by making use of the Molau's test. When formic acid was added to PA6/PP blends, the PA6 was dissolved completely within 1–3 h. The PP phase, on the other hand, separated and floated on the top [37]. This evidences the incompatibility between PA6 and PP. However, a stable emulsion in formic acid formed for MAH-g-PP compatibilized PA6/PP blends which substantiates the development of PA6-g-PP copolymer as interfacial compatibilizer.

Fig. 8(a) and (b) shows the morphology of unetched and etched fracture surface of the PA6/PP blend. In this blend, large PP particles are distributed in the continuous PA6 phase prior to formic acid etching (Fig. 8(a)). Their easy detachment from the matrix already indicates for a very weak interphase between PA6 and PP. In Fig. 8(b), most of the PA6 was dissolved in formic acid, leaving behind the PP phase that is not sensitive toward formic acid. Uncompatibilized PA6/PP blends usually show a coarse dispersion of the minor phase in the matrix owing to the inherent incompatibility [42]. The dispersed phase particles are large and irregularly shaped. Further, they possess relatively

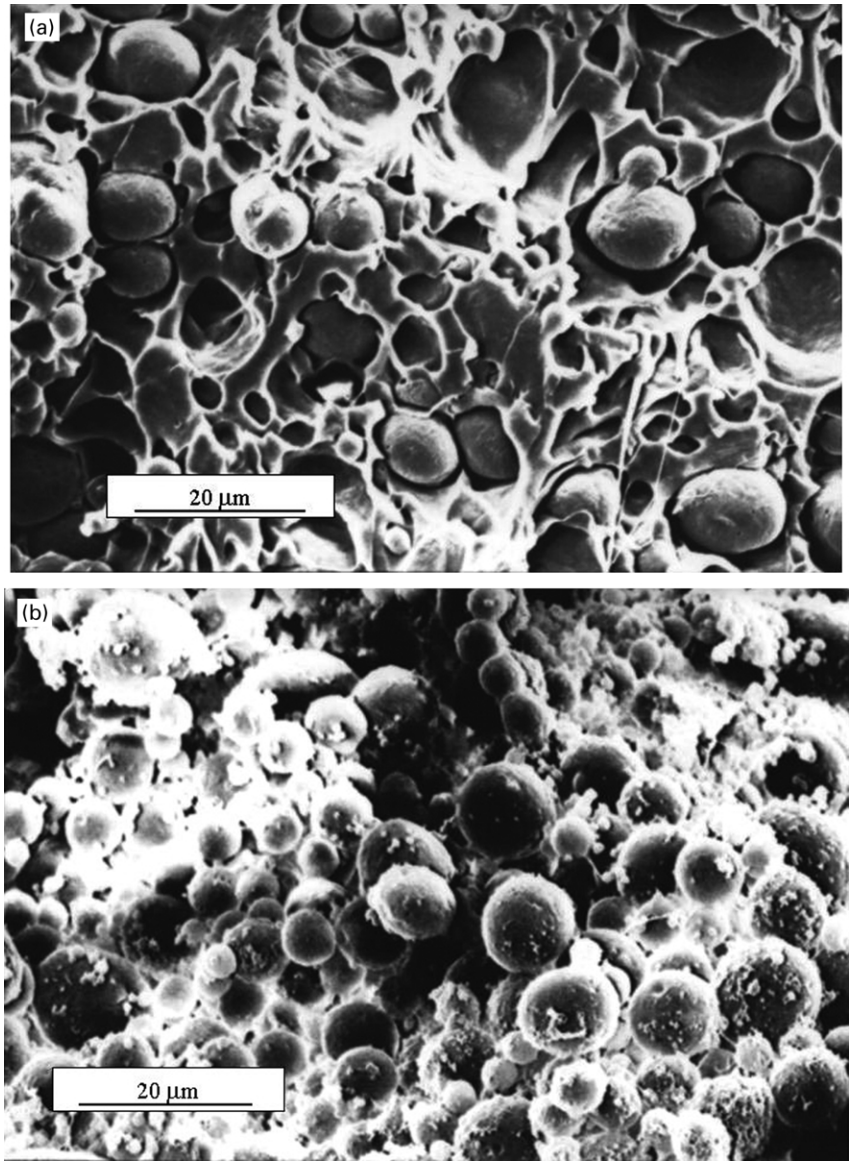

Fig. 8. (a) SEM micrograph showing the unetched surface of the PA6/PP blend. (b) SEM micrograph showing the etched (formic acid) surface of the PA6/PP blend.

small contact areas with matrix resulting in poor mechanical properties [34]. In uncompatibilized PA6/PP blends, three morphological features can be observed, i.e. droplets, fibrils, and in-between morphology of fibrils and droplets as a function of blend ratio. As the PA6 content increased, the PA6 phase turned into fibrils [46].

Fig. 9(a) and (b) shows the morphology of unetched and etched surface of the MAH-g-PP compatibilized PA6/PP/organoclay nanocomposites. The small craters in Fig. 9(a) indicate that the mean particle size of PP is substantially reduced owing to the presence of the MAH-g-PP compatibilizer. Recall that the major function of a compatibilizer is to reduce the interfacial tension between the components in the melt and thus create a finer dispersion in the blend. The interfacial bonding between PA6 and MAH-g-PP may reduce the attack by formic acid. Thus, the morphology of the etched surface of MAH-g-PP compatibilized PA6/PP nanocomposites (cf. Fig. 9(b)) is relatively similar to that of the morphology of the unetched surface (cf. Fig. 9(a)). The morphology of the ternary blends of PA6/PP/MAH-g-PP looks very homogeneous, indicating a strong interaction and adhesion between the PA6 and PP phases due to the reactive compatibilization with MAH-g-PP.

It is of interest to study the effect of morphology also on the fracture behavior. The uncompatibilized PA6/PP/organoclay nanocomposites failed brittlely (cf. Fig. 10). In the SEM micrograph taken from the fracture surface, irregular shaped, large PP particles dispersed in the PA6 matrix can

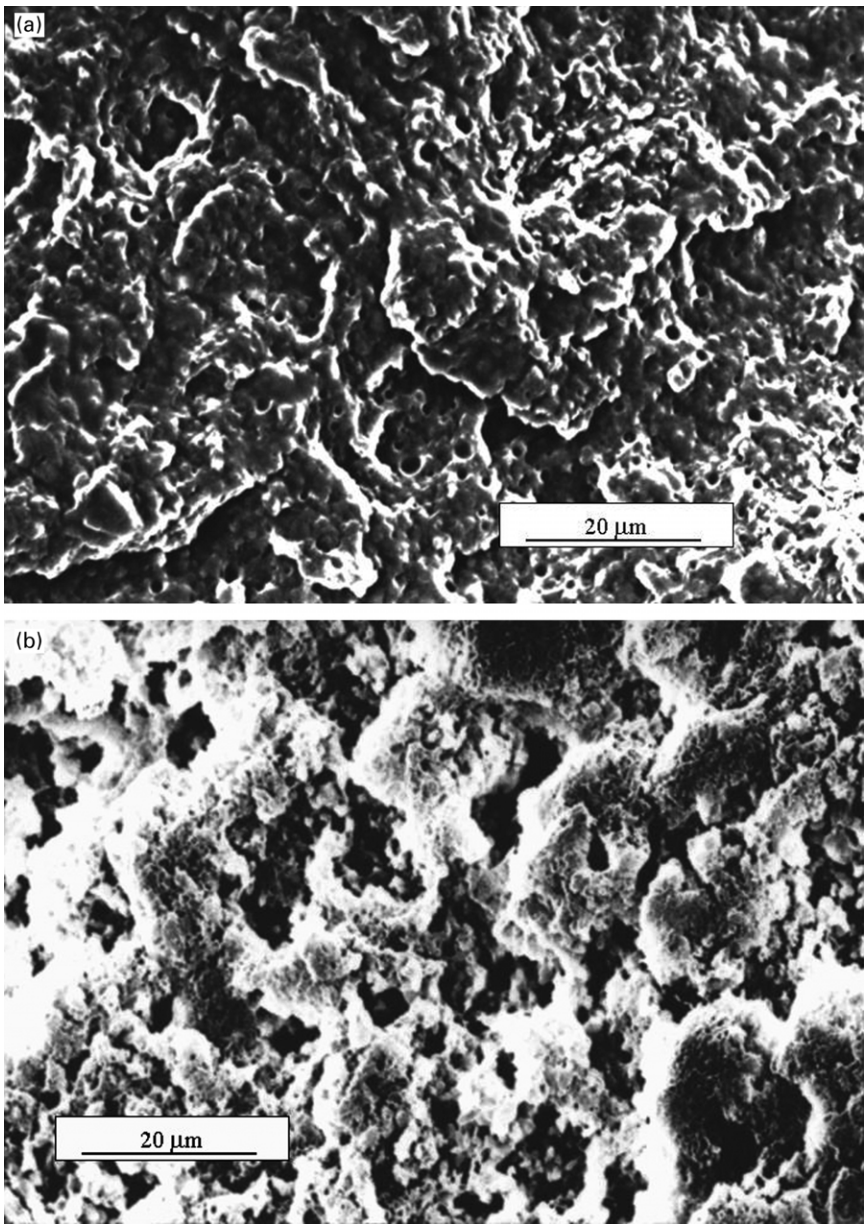

Fig. 9. (a) SEM micrograph showing the unetched surface of MAH-g-PP compatibilized PA6/PP/organoclay nanocomposite (PA6/PP/5M/4TC). (b) SEM micrograph showing the etched (formic acid) surface of MAH-g-PP compatibilized PA6/PP/organoclay nanocomposite (PA6/PP/5M/4TC).

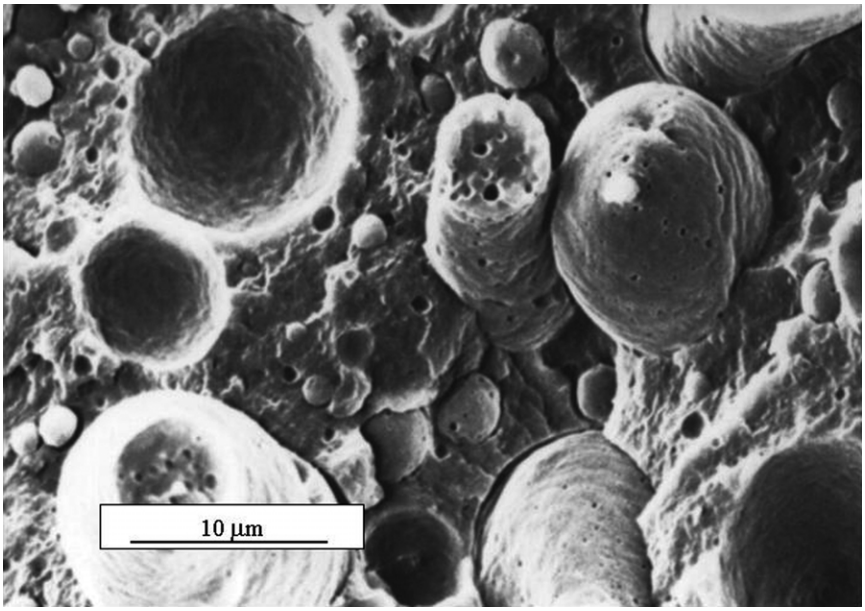

Fig. 10. SEM micrograph showing the tensile fracture surface of PA6/PP/organoclay nanocomposite.

be seen. These particles easy debond from the PA6 matrix due to the lacking interfacial adhesion. Incorporation of the organoclay alone does not produce a finer morphology in the PA6/PP blends. This explains the limited improvement in the mechanical properties noticed for the uncompatibilized nanocomposites (cf. Table 2). Fig. 11 shows the change in the failure mode due to compatibilization. The fracture surface in Fig. 11 is of ductile nature. The PP particles are markedly smaller and show a narrow particle size distribution. They act as stress concentrators in the PA6 matrix, which fails in a very ductile manner. Ductile failure is promoted by the small interparticle distance due to which plane stress condition prevails. The observed fibrillation of the matrix is caused by debonding of the PP particles followed by extensive drawing of the PA6 ligaments in between. This is the explanation for the onset of necking and improved ductility reported (cf. elongation at break values in Table 2). Furthermore, the compatibilizer located in the interphase may act as a 'bridge' between the phases and thus enhancing the loadability of the blend. It is believed that there are also interfacial interactions between the compatibilizer (MAH group) and the organoclay (octadecylamine group) in accordance to the mechanism proposed earlier (cf. Fig. 2). Thus, these interfacial interaction give rise to the synergistic effect to the strength and stiffness for the MAH-g-PP compatibilized PA6/PP nanocomposites.

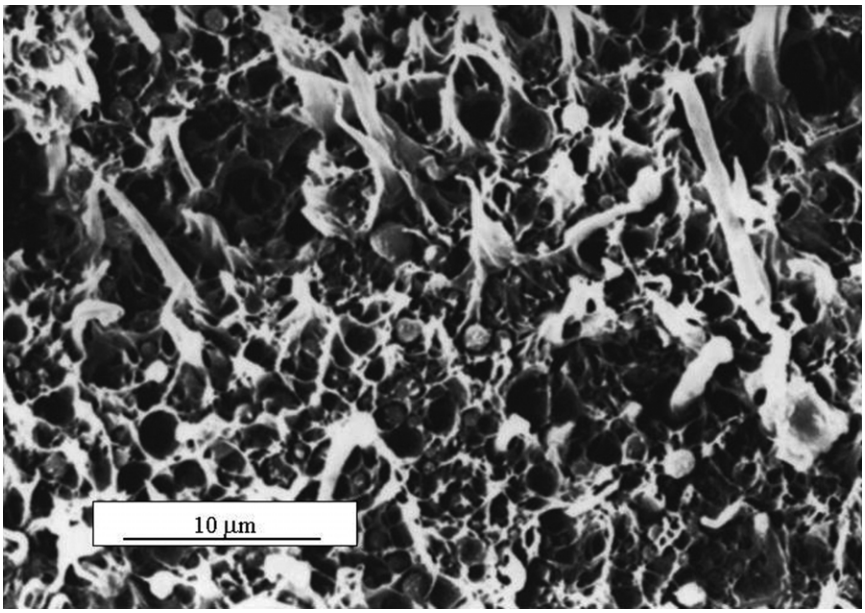

Fig. 11. SEM micrograph showing the tensile fracture surface of MAH-g-PP compatibilized PA6/PP/organoclay nanocomposite (PA6/PP/5M/4TC).

3.8. FTIR study

FTIR was carried out to study the effects of functional groups in the organoclay with respect to potential interactions with the blend constituents. Organoclay in the as received state exhibited the following absorption bands: N–H stretching at 3253 cm^{-1} aliphatic primary amines at 3400–3330 and 3330–3250 cm^{-1} [47], aliphatic C–H stretching at 2918 and 2850 cm^{-1}. The appearance of these bands are in line with the octadecylamine intercalation of the montmorillonite. The primary amine group of the octadecylamine is believed to be compatible with the PA6, which also contain amine end groups and thus may participate also in hydrogen bond formation. The proposed mechanism for the H-bonding was disclosed in Fig. 2. Thus, it is quite reasonable to suppose that the organoclay has higher affinity to the PA6 phase than to PP. This has been supported by the TEM images. It is interesting to note that an absorption band at 1032 cm^{-1} was observed in some nanocomposites. According to Huang et al. [21], this band is characteristic of sodium montmorillonite (Na-MMT). One can thus suppose that the cation exchange capacity of the montmorillonite used was not fully exploited.

3.9. Proposed morphology

Fig. 12 shows a schematic representation of the morphology of the MAH-g-PP compatibilized PA6/PP nanocomposites containing 4 phr organoclay. This scheme is proposed based on the collective evidences derived from TEM, SEM, EDX and XRD techniques. The proposed morphology shows exfoliated silicate layers distributed in the PA6 phase. However, there are also some layered silicate agglomerates which coexist with the exfoliated and intercalated ones in the PA6 phase. The mean particle size of PP (droplets) is smaller in the presence of the MAH-g-PP compatibilizer than in its absence. Thus, the MAH-g-PP acts as an effective compatibilizer by forming PA6-g-PP copolymer, as indicated in the scheme. The scheme in Fig. 12 also indicates the interaction between the amine group of octadecylamine intercalant of the exfoliated organoclay and amide groups of the PA6 and PA6-g-PP copolymer.

4. Conclusions

Based on this work devoted to study the effect of MAH-g-PP compatibilizer on the properties of PA6/PP

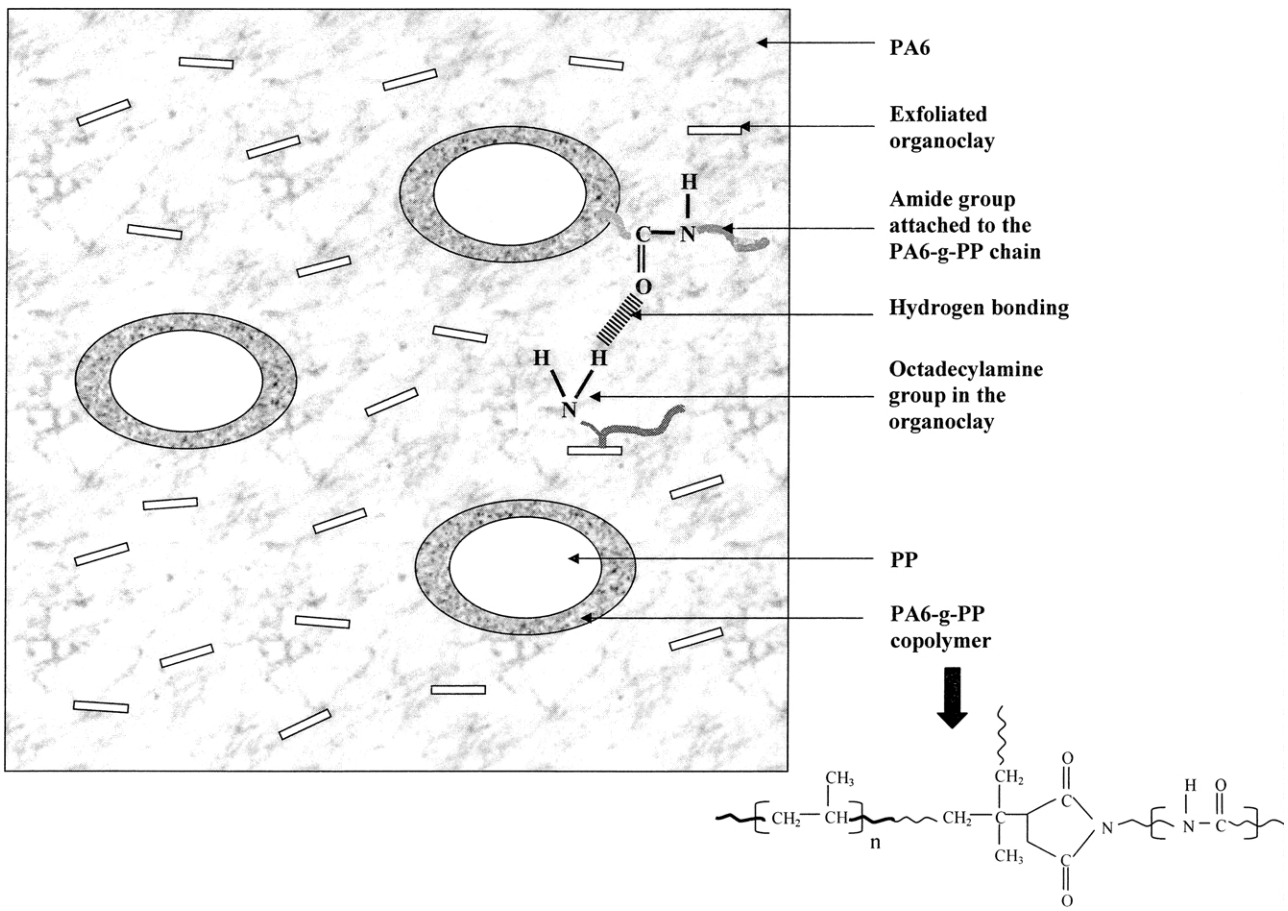

Fig. 12. Morphology sketch of MAH-g-PP compatibilized PA6/PP/organoclay nanocomposites.

(70/30 wt%) blends containing 4 phr octadecylamine intercalated montmorillonite (organoclay), the following conclusions can be drawn

4.1. Properties

Adding compatibilizer to the blend decreased the MFI value and increased the strength and ductility parameters. This was attributed to the generation of a grafted copolymer (PA6-g-PP) which formed an interphase between PA6 and PP. Incorporation of organoclay improved the stiffness and reduced the ductility, as expected, for its exfoliation and intercalation. The presence of organoclay slightly affected the degree of crystallinity of the PA6 phase and its crystallization behavior.

4.2. Morphology

The coarse dispersion of PP became markedly finer owing to the compatibilizer MAH-g-PP. The organoclay was partly exfoliated (shown by TEM), partly intercalated (based on TEM and XRD) and partly aggregated (revealed by SEM) and preferentially located in the PA6 and PA6-g-PP phases of the blends. It was speculated that H-bonding between the amine groups of the octadecylamine intercalant of the clay and carbonyl groups of the PA6 and PA6-g-PP favours the exfoliation of the organoclay.

Acknowledgements

The authors would like to thank Ministry of Science, Technology and Environment (MOSTE), Malaysia for the IRPA grant (grant no: 063171/IRPA). Special scholarship granted by Universiti Sains Malaysia to one of us (Mr W.S. Chow) is gratefully acknowledged. We also thank to Dr R. Thomann (Freiburg, Germany) for performing the TEM measurements.

References

[1] Folkes MJ, Hope PS. Polymer blends and alloys. London: Chapman and Hall; 1993.
[2] Holsti-Miettinen RM, Perttila KP, Seppälä JV, Heino MT. J Appl Polym Sci 1995;58:1551.
[3] Lee JW, Lim YT, Park OO. Polym Bull 2000;45:191.
[4] Zanetti M, Lomakin S, Camino G. Macromol Mater Engng 2000;279:1.
[5] Wang H, Elkovitch M, Lee LJ, Koelling KW, ANTEC2000, May 7–11, vol. II. New York: Society of Plastics Engineers; 2000. p. 2402.
[6] Kawasumi M, Hasegawa N, Kato M, Usuki A, Okada A. Macromolecules 1997;30:6333.
[7] Reichert P, Nitz H, Klinke S, Brandsch R, Thomann R, Mülhaupt R. Macromol Mater Engng 2000;275:8.
[8] Hambir S, Bulakh N, Kodgire P, Kalgaonkar R, Jog JP. J Polym Sci Part B: Polym Phys 2001;39:446.
[9] Reichert P, Hoffmann B, Bock T, Thomann R, Mülhaupt R, Friedrich C. Macromol Rapid Commun 2001;22:519.
[10] Solomon MJ, Almusallam AS, Seefeldt KF, Somwangthanaroj A, Varadan P. Macromolecules 2001;34:1864.
[11] Zanetti M, Camino G, Reichert P, Mülhaupt R. Macromol Rapid Commun 2001;22:176.
[12] Shelley JS, Mather PT, DeVries KL. Polymer 2001;42:5849.
[13] Cho JW, Paul DR. Polymer 2001;42:1083.
[14] Kojima Y, Usuki A, Kawasumi M, Okada A, Kurauchi T, Kamigaito O. J Polym Sci Part A: Polym Chem 1993;31:983.
[15] Fong H, Vaia RA, Sanders JH, Lincoln D, John PJ, Vreugdenhil AJ, Bultman J, Cerbus CA, Jeon HG. Polym Prepr 2001;42:354.
[16] Lincoln DM, Vaia RA. Polym Prepr 2001;42:55.
[17] Sikka M, Cerini LN, Ghosh SS, Winey KI. J Polym Sci Part B: Polym Phys 1996;34:1443.
[18] Hoffmann B, Dietrich C, Thomann R, Friedrich C, Mülhaupt R. Macrmol Rapid Commun 2000;21:57.
[19] Park CI, Park OO, Lim JG, Kim HJ. Polymer 2001;42:7465.
[20] Hsiao SH, Liou GS, Chang LM. J Appl Polym Sci 2001;80:2067.
[21] Huang JC, Zhu ZK, Ma XD, Qian XF, Yin J. J Mater Sci 2001;36:871.
[22] Yano K, Usuki A, Okada A, Kurauchi T, Kamigaito O. J Polym Sci Part A: Polym Chem 1993;31:2493.
[23] Chin IJ, Thurn-Albrecht T, Kim HC. Polym Prepr 2000;41:591.
[24] Curliss DB. Polym Prepr 2000;41:523.
[25] Kornmann X, Lindberg H, Berglund LA. Polymer 2001;42:1303.
[26] Jiang GJ, Tsai HY. Polym Prepr 2000;41:621.
[27] Huang XY, Brittain WJ. Polym Prepr 2000;41:521.
[28] Kornmann X, Berglund LA, Sterte J, Giannelis EP. Polym Engng Sci 1998;38:1351.
[29] Jimenez G, Ogata N, Kawai H, Ogihara T. J Appl Polym Sci 1997;64:2211.
[30] Choi HJ, Kim SG, Hyun YH, John MS, Polym Prepr 2000 41: 1183.
[31] Huang XY, Lewis S, Brittain WJ, Vaia RA. Polym Prepr 2000;41:589.
[32] Chow WS, Ishiaku US, Mohd. Ishak ZA, Karger-Kocsis J, Apostolov AA. J Appl Polym Sci, accepted for publication.
[33] Ide F, Hasegawa A. J Appl Polym Sci 1974;18:963.
[34] Sathe SN, Devi S, Srinivasa Rao GS, Rao KV. J Appl Polym Sci 1996;61:97.
[35] Sathe SN, Srinivasa Rao GS, Rao KV, Devi S. Polym Engng Sci 1996;36:2443.
[36] González-Montiel A, Keskkula H, Paul DR. Polymer 1995;36:4587.
[37] Molau GE. J Polym Sci 1995;A3:4235.
[38] Coran AY, Patel R, Williame HD. Rubber Chem Technol 1985;58:1014.
[39] Marco C, Ellis G, Gómez MA, Fatou JG, Arribas JM, Campoy I, Fontecha A. J Appl Polym Sci 1997;65:2665.
[40] Rösch J, Mülhaupt R. J Appl Polym Sci 1995;56:1599.
[41] Campoy I, Arribas JM, Zaporta MAM, Marco C, Gómez MA, Fatou JG. Eur Polym J 1995;31:475.
[42] Lee JD, Yang SM. Polym Engng Sci 1995;35:1821.
[43] Park SJ, Kim BK, Jeong HM. Eur Polym J 1990;26:131.
[44] Datta RK, Polk MB, Kumar S. Polym-Plast Technol Engng 1995;34:551.
[45] Baer E, Radcliffe SV. Polymeric materials: relationships between structure and mechanical behavior. USA: American Society for Metals; 1975.
[46] Azhari CH, Jamil IM, Rohani MR. National symposium polymeric materials: development in polyamide thermoplastic composites 2001; 2001.
[47] Silverstein RM, Bassler GC, Morrill TC. Spectrometric identification of organic compounds. New York: Wiley; 1991.
[48] Liu X, Wu Q, Berglund LA, Fan J, Qi Z. Polymer 2001;42:8235.
[49] Aklonis JJ, MacKnight WJ. Introduction to polymer viscoelasticity, 2nd ed. New York: Wiley; 1983.
[50] Progelhof RC, Throne JL. Polymer engineering principles: properties, processes and test for design. New York: Hanser; 1993.
[51] Mohd Ishak ZA, Berry JP. J Appl Polym Sci 1994;51:2145.
[52] Wu Z, Zhou C, Qi R, Zhang H. J Appl Polym Sci 2002;83:2403.